ELSEVIER

Available online at www.sciencedirect.com

SCIENCE DIRECT®

International Journal of Solids and Structures 43 (2006) 5355–5369

INTERNATIONAL JOURNAL OF SOLIDS and STRUCTURES

www.elsevier.com/locate/ijsolstr

Inner mass impact damper for attenuating structure vibration

Jianlian Cheng *, Hui Xu

Department of Engineering Mechanics, School of Architecture and Mechanics, Xi'an Jiaotong University, Xi'an 710049, PR China

Received 22 April 2005
Available online 21 September 2005

Abstract

The behaviors of a vibration system suppressed with an impact damper are investigated, where the impact damper is simplified as a combination of spring and viscous damping. The analytical theory for the optimal impact control algorithms for impact damper is developed, and the accurate expressions are derived for the optimal values of the impact damper damping and initial displacement in a single-degree-of-freedom structure. The relation between coefficient of restitution and impact damping ratio is obtained. The investigation shows that the effective reduction of the vibration response is nearly independent of the number of impacts, but primarily related to the type of collision which the impact mass collides with the main mass face-to-face. This theory is generalized to continuous structures. An example of an impact damper in a rotating cantilever beam demonstrates that the impact dampers are suitable for attenuating the impulse response of structures unconditional stable without the requirement of the accuracy of the modal information.

Keywords: Impact damper; Optimal initial displacement; Coefficient of restitution; Vibration response

1. Introduction

Applications of impact damper to attenuate the undesirable structure vibration, such as turbine blades, and high-speed railway bridge, robot arms and so on, have been investigated analytically, numerically and experimentally for many years (Dlmentberg and Iourtchenko, 2004; Ema and Marui, 1996; Cheng and Shiu, 2001; Carotti and Turci, 1999; Zhang and Angeles, 2005). Cheng and Wang (2003) discussed the behaviors of a resilient impact damper in free damped vibration, and the results showed that the clearance between two masses in an effect impact damper ought to be smaller than twice of the initial displacement of the main mass in a vibration system if the system is stimulated by an initial displacement only. Ema and

* Corresponding author.
E-mail address: cheng19690912@163.com (J. Cheng).

0020-7683/$ - see front matter
doi:10.1016/j.ijsolstr.2005.07.026

Marui (1996) investigated analytically and experimentally the characteristics of an impact damper in free damped vibration in detail, and they indicated that the damping capability of the vibratory system could be improved at least eightfold using a proper impact damper. Collette (1998) researched vibration control capability of a combined tuned absorber and impact damper under a random excitation, and analyzed the effectiveness of the optimally combined absorber and its sensitivity to variations of the clearance, restitution coefficient and the mass ratio between the impact damper and absorber.

Usually, an effective reduction of the excessive oscillations can be obtained by the well-known tuned mass damper (TMD) (Joshi and Jangid, 1997). The TMD is successfully used in several civil engineering structures, such as towers and bridges (Wang et al., 2003), where viscous damping of the TMD is introduced with different hydraulic mechanisms. Therefore, if we want to acquire a desired damping, it is extremely complicated for during a mechanism of suppressing vibration continual maintenance. The impact damper usually is a mass placed inside the structure and holds a small clearance to the structure. When the displacement of the primary system exceeds the clearance, the impact mass collides with the container wall companying with energy dissipation and momentum exchange. Sometimes, energy dissipation is helpful in attenuating the excessive vibration amplitudes of the primary structure, but the momentum exchange obviously facilitates controlling the amplitudes during collisions. The direction of motion of the smaller impact mass is reversed after a collision, whereas the velocity of the primary structure is only reduced due to its larger inertia. As a result, the primary system attains smaller displacement amplitude than that in the situation without impacts. For the modeling of impact damper on a vibratory system, it is necessary to derive lot of formulas for the steady-state response with two symmetric impacts per cycle or arbitrary number of impacts under sinusoidal excitation (Barbara, 2001; Janin and Lamarque, 2001; Yao et al., 2005). At present, most of the dynamic characteristic investigations of impact dampers assume that the impact condition between the impact damper and the primary system is governed by the coefficient of restitution, which results in discontinuity in the phase plane. The contact time, defined as the impact damper stays in contact with the main mass, is neglected, and collision usually produces high-frequency noise in practice. Although the impact damper has been investigated for a long time, there are still two fundamental issues that need to be clearly addressed. One is what the main damping mechanism of the impact damper is; and another is how to determine the clearance that effectively suppresses the response of the vibratory system.

In this paper, a simple model of impact damper is established as a combination of spring and viscous damper. The explicit expressions are obtained for the optimal initial displacement of the impact damper and damping ratio via analyzing the course of the collision. The relation between the impact coefficient of restitution and damping ratio is obtained. An experimental cantilever beam for simulating rotating motion of robot arm where a mass damper is mounted inside, is constructed to verify the availability of the theoretical analysis.

2. Structure model

To conveniently analyze the dynamic characteristics of impact damper vibration system, a model with two-degrees-of-freedom as shown in Fig. 1 is considered. The impacts are modeled by two linear contact springs and the dampers, each of stiffness K_1 and damping factor c_1. However, the friction force between M and m is neglected. The motion of the system can be treated as a piecewise linear process (Lamarque and Janin, 2000).

When $x_2(t) - x_1(t) > d/2$ (or $x_2(t) - x_1(t) < -d/2$), the impact mass collides with the left (or right) side of the main mass so the equation of motion is expressed as

$$\begin{bmatrix} M & 0 \\ 0 & m \end{bmatrix} \begin{Bmatrix} \ddot{x}_1 \\ \ddot{x}_2 \end{Bmatrix} + \begin{bmatrix} c + c_1 & -c_1 \\ -c_1 & c_1 \end{bmatrix} \begin{Bmatrix} \dot{x}_1 \\ \dot{x}_2 \end{Bmatrix} + \begin{bmatrix} k + k_1 & -k_1 \\ -k_1 & k_1 \end{bmatrix} \begin{Bmatrix} x_1 \\ x_2 \end{Bmatrix} = 0 \tag{1}$$

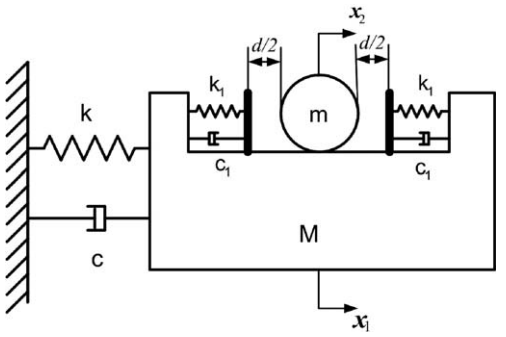

Fig. 1. Schematic diagram of model.

When $-d/2 \leqslant x_2(t) - x_1(t) \leqslant d/2$, the impact mass moves freely at a constant speed without causing any collision; therefore, the motion are given by

$$M\ddot{x}_1 + c\dot{x}_1 + kx_1 = 0, \quad m\ddot{x}_2 = 0 \tag{2a, b}$$

The collisions are idealized as discontinuous processes governed by the conservation of momentum and the definition of the coefficient of restitution ($\alpha < 1$). The velocity of M and m just before and immediately after a collision are thereby related by the equations

$$\dot{x}_1^+ = \frac{(1-\mu\alpha)}{(1+\mu)}\dot{x}_1^- + \frac{\mu(1+\alpha)}{1+\mu}\dot{x}_2^-, \quad \dot{x}_2^+ = \frac{(1+\alpha)}{(1+\mu)}\dot{x}_1^- + \frac{(\mu-\alpha)}{(1+\mu)}\dot{x}_2^- \tag{3}$$

where $\mu = m/M$ is the mass ratio. The restitution coefficient α is defined by

$$\alpha = -(\dot{x}_2^+ - \dot{x}_1^+)/(\dot{x}_2^- - \dot{x}_1^-) \tag{4}$$

The superscripts $-$ and $+$ refer to states just before and immediately after a collision, respectively.

When the impact mass collides with the main mass during vibration, an impulse force acts both on them as shown in Fig. 2. The impact mass, because of its elasticity, has a local strain at the contact point that we model by a spring. Especially, the damping capacity of the vibratory system is mainly produced in the contacting surface and is assumed to be viscous. Therefore, the impact interface between the impact main and the main mass is modeled using a spring and a damper. Based on Eq. (1), the motion equations of the free mass colliding with the main mass become

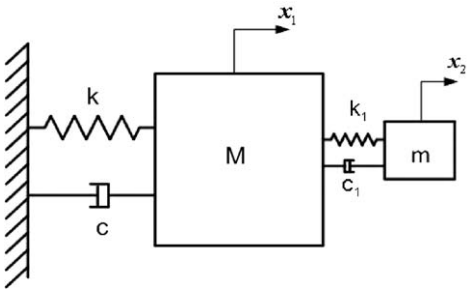

Fig. 2. Schematic while the impact damper colliding the main mass.

$$\ddot{x}_1(t) + 2\zeta\omega\dot{x}_1(t) + \omega^2 x_1(t) = \mu[2\zeta_1\omega_1\dot{y}(t) + \omega_1^2 y(t)] \tag{5}$$

$$\ddot{y}(t) + 2\zeta_1\omega_1\dot{y}(t) + \omega_1^2 y(t) = -\ddot{x}_1(t) \tag{6}$$

where $\omega = \sqrt{k/M}$, $\omega_1 = \sqrt{k_1/m}$, $\zeta = \frac{c}{2M\omega}$, $\zeta_1 = \frac{c_1}{2m\omega_1}$, $y(t) = x_2(t) - x_1(t)$, $\mu = m/M$.

At time $t = 0$ the system has initial conditions

$$x_1(0) = x_{10}, \quad x_2(0) = x_{20}, \quad y(0) = y_0 = x_{20} - x_{10},$$
$$\dot{x}_1(0) = \dot{x}_{10}, \quad \dot{x}_2(0) = \dot{x}_{20}, \quad \dot{y}(0) = \dot{y}_0 = \dot{x}_{20} - \dot{x}_{10}.$$

First, using the Laplace transform, Eqs. (5) and (6) become

$$\begin{aligned} d(s)X_1(s) = {} & (s^2 + 2\zeta_1\omega_1 + \omega_1^2)(s\dot{x}_{10} + x_{10} + 2\zeta\omega x_{10} - 2\mu\zeta_1\omega_1 y_0) \\ & + (2\mu\zeta_1\omega_1 s + \omega_1^2)(s\dot{y}_0 + y_0 + 2\zeta_1\omega_1 y_0 + s\dot{x}_{10} + x_{10}) \end{aligned} \tag{7}$$

$$\begin{aligned} d(s)Y(s) = {} & (s^2 + 2\zeta\omega + \omega^2)(s\dot{y}_0 + y_0 + 2\zeta_1\omega_1 y_0 + s\dot{x}_{10} + x_{10}) \\ & - s^2(s\dot{x}_{10} + x_{10} + 2\zeta\omega x_{10} - 2\mu\zeta_1\omega_1 y_0) \end{aligned} \tag{8}$$

where $X_1(s)$ and $Y(s)$ are the transforms of the main mass and impact damper responses, $x_1(t)$ and $y(t)$.

In the following, a perturbation solution to the system free vibration response is presented. The derivations are based on the following assumption: (1) the impact damper is tuned or nearly tuned to the structure, so that the natural frequencies can be approximated by their average, $\omega \approx \omega_1 \approx \omega_a = (\omega + \omega_1)/2$. Thus, the equations of motion are slightly simplified; (2) the impact mass is small compared to the main mass; (3) the main mass damping ratio is small relative to the impact damper damping ratio. These assumptions are satisfied for most structure impact damper systems. In particular, the last assumption is not restrictive because vibration control would not be needed for a highly damped structure. From these assumptions, there are two small perturbation parameters: the impact damper damping ratio, ζ_1, and the ratio of masses, $\mu \equiv m/M$.

Based on forenamed assumptions, the equations of motion are slightly simplified. The natural frequencies are approximated by their average, ω_a. Also the velocity term on the right side of Eq. (7) is neglected because of the relatively small damping parameter ζ appearing in the coefficient. Then, the Laplace transform is applied to the simplified equation. The solution to the simplified equations in Laplace transform space is

$$d(s)X_1(s) = (\omega_a^2 + 2\zeta_1\omega_a s + s^2 + \mu\omega_a^2)(\dot{x}_{10} + sx_{10}) + \mu\omega_a^2[\dot{y}_0 + (s + 2\zeta_1\omega_a)y_0] \tag{9}$$

$$d(s)Y(s) = \omega_a^2(\dot{x}_{10} + sx_{10}) + (\omega_a^2 + s^2)[\dot{y}_0 + (s + 2\zeta_1\omega_a)y_0] \tag{10}$$

$d(s)$ is the characteristic polynomial of the system:

$$d(s) = (s^2 + \omega_a^2)(\omega_a^2 + 2\zeta_1\omega_a s + s^2) + \mu\omega_a^2 s^2 \tag{11}$$

By setting $d(s) = 0$, we can obtain the four characteristic roots as follows:

$$\begin{aligned} s_{1,2} &= -\frac{1}{2}\zeta_1\omega_a \pm \frac{1}{2}\sqrt{-\mu\omega_a^2 + \zeta_1^2\omega_a^2} + \frac{1}{2}\sqrt{\left(-4\omega_a^2 - \mu\omega_a^2 + 2\zeta_1^2\omega_a^2 + \frac{2\mu\zeta_1\omega_a^3 - 2\zeta_1^3\omega_a^3}{\sqrt{-\mu\omega_a^2 + \zeta_1^2\omega_a^2}}\right)} \\ s_{3,4} &= -\frac{1}{2}\zeta_1\omega_a \pm \frac{1}{2}\sqrt{-\mu\omega_a^2 + \zeta_1^2\omega_a^2} - \frac{1}{2}\sqrt{\left(-4\omega_a^2 - \mu\omega_a^2 + 2\zeta_1^2\omega_a^2 + \frac{2\mu\zeta_1\omega_a^3 - 2\zeta_1^3\omega_a^3}{\sqrt{-\mu\omega_a^2 + \zeta_1^2\omega_a^2}}\right)} \end{aligned} \tag{12}$$

To evaluate the inverse Laplace transform, four roots of the polynomial $d(s)$ are needed. Although the exact roots can be used, the resulting expressions are too complicated to provide any insight into the system. An alternative is to use the small perturbation parameters and derive approximate roots. The latter approach is used here (Igusa et al., 1985 and Fujino and Abe, 1993). Since the damping ratio ζ_1 and the mass ratio μ are small values, those high-order minor terms can be neglected. The four approximate roots of the characteristic polynomial are obtained. These roots are given as follows:

$$s_1, s_2 = \omega_a\left(-\frac{\zeta_1 \pm \sqrt{\zeta_1^2-\mu}}{2} + j\right), \quad s_3, s_4 = \omega_a\left(-\frac{\zeta_1 \pm \sqrt{\zeta_1^2-\mu}}{2} - j\right) \tag{13}$$

where $j \equiv \sqrt{-1}$. The four poles are distinct except for the special case of $\zeta_1 = \sqrt{\mu}$.

Now, we return to the initial status. The impact mass has a local strain at contact point that we model by a spring and a viscous damper. Since the motion of the system can be treated as a piecewise linear process, we need to consider three cases as the following:

Case I: When $y(t) > d/2$, Eq. (1) is used. The corresponding responses are given (Eberhard and Hu, 2003):

$$x_1(t) = \sum_i^4 r_i P^{(i)} e^{s_i t}, \quad x_2(t) = \sum_i^4 P^{(i)} e^{s_i t} \tag{14}$$

where $r_i = \frac{c_1 s_i + k_1}{M s_i + (c+c_1)s_i + (k+k_1)}$ for $i = 1, 2, 3, 4$ and s_i ($i = 1, 2, 3, 4$) are the characteristic roots of system shown in Eq. (13). The functions $P^{(i)}$ ($i = 1, 2, 3, 4$) are determined by the initial conditions of the system.

Based on Eq. (13), we may consider three cases to express:

(1) $\zeta_1 < \sqrt{\mu}$. Here, the radical $\sqrt{\zeta_1^2-\mu}$ is a pure imaginary number. According to Eq. (13), the real parts of the poles are all equal to $\omega_a\zeta/2$. Thus from a modal viewpoint, the two system damping ratios are equal and the natural frequencies are unequal. Based on the aforementioned initial condition, the approximate solution for the structure response becomes

$$x_1(t) = A\cos\left(\frac{1}{2}\sqrt{\mu-\zeta_1^2}\omega_a t - \theta\right) e^{\left(-\frac{1}{2}\zeta_1\omega_a t\right)} \sin(\omega_a t) \tag{15}$$

where the amplitude A and phase θ are given by

$$A = \left[\left(\frac{\dot{x}_{10}}{\omega_a}\right)^2 + \left(\mu y_0 + \left(\zeta_1 + \frac{\mu}{2}\right)\frac{\dot{x}_{10}}{\omega_a}\right)^2 \left(\mu - \zeta_1^2\right)^{-1}\right]^{1/2} \tag{16a}$$

and

$$\theta = \tan^{-1}\left[\left(\frac{\mu\omega_a y_0}{\dot{x}_{10}} + \zeta_1 + \frac{\mu}{2}\right)\left(\mu-\zeta_1^2\right)^{-1/2}\right] \tag{16b}$$

(2) $\zeta_1 = \sqrt{\mu}$. Since the radical $\sqrt{\zeta_1^2-\mu}$ is zero, there are two double roots in Eq. (13), given by $s_1 = s_2 = \omega_a(j - \sqrt{\mu/2})$ and $s_3 = s_4 = \omega_a(-j - \sqrt{\mu/2})$. This particular value for the impact damping has been shown to be optimal for a certain free vibration problem. For this case, the structure response can be combined, yielding

$$x_1(t) = \left[\frac{\dot{x}_{10}}{\omega_a} + \frac{\sqrt{\mu}\dot{x}_{10} + \mu\omega_a y_0}{2} t\right] e^{-\frac{1}{2}\sqrt{\mu}\omega_a t} \sin(\omega_a t) \tag{17}$$

The exponential decay rate is $\sqrt{\mu}\omega_a/2 = \zeta_1\omega_a/2$, which is the same as in case (1). However, the slow oscillation which appeared in case (1) is now replaced by a linear function of t. This change in the response

behavior, which is due to the double poles of the system, results in a decay of the structural response that is much slower than the exponential decay rate $\zeta\omega_a/2$.

(3) $\zeta_1 > \sqrt{\mu}$. In this case, the radical $\sqrt{\zeta_1^2-\mu}$ is a pure real number and the imaginary parts of the poles are equal to $\pm\omega_a$. Thus the system damping ratios are unequal and the natural frequencies are equal. The solution of the structure response becomes

$$x_1(t) = \left\{ \left[-\mu y_0 + \left(-\zeta_1 + \sqrt{\zeta_1^2-\mu} \right) \frac{\dot{x}_{10}}{\omega_a} \right] e^{-\frac{\zeta_1+\sqrt{\zeta_1^2-\mu}}{2}\omega_a t} + \left[\mu y_0 + \left(\zeta_1 + \sqrt{\zeta_1^2-\mu} \right) \frac{\dot{x}_{10}}{\omega_a} \right] e^{\frac{-\zeta_1+\sqrt{\zeta_1^2-\mu}}{2}\omega_a t} \right\} \frac{\sin(\omega_a t)}{2\sqrt{\zeta_1^2-\mu}} \tag{18}$$

In Eq. (18), there are two exponentially decaying terms within the braces. The first has a decay rate of $(\zeta_1 + \sqrt{\zeta_1^2-\mu})\omega_a/2$, while the second has a slower decay rate of $(\zeta_1 - \sqrt{\zeta_1^2-\mu})\omega_a/2$.

Case II: When $-d/2 \leqslant y(t) \leqslant d/2$, the impact mass freely at a constant speed without causing any collision. The equations of motion are presented by Eqs. (2a) and (2b). Therefore, the motions are given by

$$x_1(t) = e^{-\zeta\omega t}\left[x_{10}\cos(\omega_d t) + \frac{\dot{x}_{10} + \zeta\omega x_{10}}{\omega_d}\sin(\omega_d t) \right] \tag{19}$$

$$x_2(t) = \dot{x}_{20} t + x_{20} \tag{20}$$

where $\omega_d = \sqrt{1-\zeta^2}\omega$ and $x_{10}, \dot{x}_{10}, x_{20}, \dot{x}_{20}$ are the initial displacements and velocities for the impact damper and main mass, respectively.

Case III: When $y(t) < -d/2$, the impact mass collides with the right side of the main mass. The structure responses have the same forms as Eqs. (15)–(18), which we assume that spring and damping coefficient of the right side is the same as ones of the left side.

3. Parameters sensitivity analysis and the effect of application

3.1. Influence of initial displacement and numerical simulations

In the foregoing mention, the initial condition $x_{10} = 0$, $\dot{x}_{10} \neq 0$, $x_{20} = 0$, $\dot{x}_{20} \neq 0$ as well as $y_0 = 0$, $\dot{y}_0 \neq 0$ at $t = 0$, are substituted into the response expressions. We assume that the impact mass is fixed relative the main mass for $t \leqslant 0$. Immediately after the impact, the impact mass is released. The structure response is nearly relative to the impact mass initial displacement.

When $\zeta_1^2 < \mu$, we can see from Eq. (16a) that the amplitude A is minimized with respect to y_0 when $\mu y_0 + (\zeta_1 + \mu/2)\dot{x}_{10}/\omega_a = 0$, i.e. $y_0^* = -(\zeta_1 + \mu/2)\dot{x}_{10}/\mu\omega_a$. Thus the optimal initial displacement is

$$x_{20}^* = y_0^* = -\left(\zeta_1 + \frac{\mu}{2}\right)\dot{x}_{10}/\mu\omega_a \tag{21}$$

Here, the corresponding main mass response has the same low oscillation and exponential decay as the original response, but with smaller amplitude and zero phases.

When $\zeta_1^2 = \mu$, in Eq. (17), the main mass response amplitude is a variable by time t. The coefficient $(\sqrt{\mu}\dot{x}_{10} + \mu\omega_a y_0)t/2$ can be eliminate when $\sqrt{\mu}\dot{x}_{10} + \mu\omega_a y_0 = 0$. The impact mass initial displacement

$$x_{20}^* = y_0^* = -\dot{x}_{10}/\sqrt{\mu}\omega_a \tag{22}$$

When $\zeta_1^2 > \mu$, in Eq. (18), within the braces two exponentially decaying terms, the latter has a slower decay. Thus, we consider the effect of the second term, with the initial impact mass displacement

$$x_{20}^{*} = -\frac{\zeta_1 + \sqrt{\zeta_1^2 - \mu}}{\mu\omega_a}\dot{x}_{10} \tag{23}$$

To illustrate the results of this impact, numerical simulations are presented for a structure impact system and mass ratio $\mu = 0.01$. The normalized structural response used herein is the square root of the structural energy divided by the initial structural energy, $\sqrt{E(t)/E_0}$, where $E(t) = M[\dot{x}_1^2(t) + \omega_a^2 x_1^2(t)]/2$ and $E_0 = M\dot{x}_{10}^2/2$. The time history of the normalized structural responses are plotted in Fig. 3 for both $x_{20} = 0$ and $x_{20} = x_{20}^{*}$, to show the effect of the initial displacements. Three impact damping ratios are considered $\zeta_1 = 0.05, 0.1, 0.3$. For Case I in Fig. 3, the responses of the main mass with and without the optimal value for initial displacement x_{20} are shown. It is clearly found that the amplitude of $x_{20} = 0$ is larger than one of the optimal value. From Fig. 3 shown, the phases are different to two types of the initial displacement. According to Eq. (17), corresponding to the case II in Fig. 3, the responses of the structure with different initial displacement exponentially decay at the rate $0.05\omega_a$. This response is smaller than that of the structure with $x_{20} = 0$, since the term with the factor t in Eq. (17) vanishes when $x_{20} = x_{20}^{*}$. And for the case III, the responses are shown for $\zeta_1 = 0.3$. It is obvious that the effects of reducing vibration are distinct when $x_{20} = 0$ than when $x_{20} = x_{20}^{*}$. This behavior can be explained by the expressions for the structure response exponential decay. When $x_{20} = 0$, Eq. (18) shows that the exponential decay rate is $(\zeta_1 - \sqrt{\zeta_1 - \mu})\omega_a/2$. However, when the initial displacement is the optimal value, the second term within the brace in Eq. (18) is zero, which the exponential decay rate is an increasing function of ζ_1. Therefore, if the initial displacement can be chosen as its optimal value, the impact damping ratio should be set as high as possible. In particular, for small mass ratios, μ, and relatively large damping ratios, ζ_1, the vibration attenuation can be extremely effective.

3.2. Effect of the restitution coefficient and the clearance to reduce the vibration response

Based on the previous results, the number of collisions is not the main reason that causes the vibration reduction. The crucial momentum exchange by the impact damper during impacts should be the collision that occurs while the impact mass and the main mass are moving toward each other. Therefore, an effective

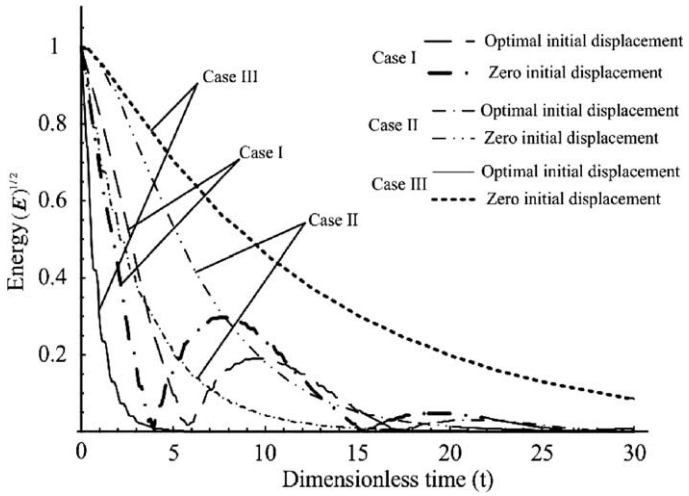

Fig. 3. The results of impact mass initial displacement to main mass response.

impact damper is determined by the coefficient of restitution and a proper clearance when the impact mass collides with the main mass face-to-face.

Now, we consider that the impact mass collides with the left side of the main mass and assume that the spring and damping of the main mass may be neglected at this moment for simplicity. Since the forces acting on the masses are internal, the equation of motion of the whole system reduces to $M\ddot{x}_1 + m\ddot{x}_2 = 0$. Using the relation $\ddot{y} = \ddot{x}_2 - \ddot{x}_1$, the accelerations of the masses can be expressed in terms of $\ddot{y}$ as $\ddot{x}_1 = [\mu/(1+\mu)]\ddot{y}$ and $\ddot{x}_2 = -[1/(1+\mu)]\ddot{y}$. The equations of motion (5) and (6) are simplified as

$$\ddot{y}(t) + 2\zeta_1\omega_1(1+\mu)\dot{y}(t) + \omega_1^2(1+\mu)y(t) = 0 \tag{24}$$

where $y(t) = x_2(t) - x_1(t)$ is the position of the mass main relative to the impact mass.

For the solution of this equation, the initial conditions can be expressed as $y_0(0) = 0$, $\dot{y}_0(0) = \dot{y}_0^+$ where $\dot{y}_0^+$ denotes the relative velocity before the collision occurs. Substituting the initial condition into Eq. (24), the displacements can be yield

$$y(t) = \begin{cases} \dfrac{\dot{y}_0^+ \exp[-\zeta_1\omega_1(1+\mu)t]\sin\left(\sqrt{1+\mu-\zeta_1^2(1+\mu)^2}\,\omega_1 t\right)}{\sqrt{1+\mu-\zeta_1^2(1+\mu)^2}\,\omega_1}, & \zeta_1\sqrt{1+\mu} < 1 \\ \dot{y}_0^+ t\exp[-\omega_1(1+\mu)t], & \zeta_1\sqrt{1+\mu} = 1 \\ \dfrac{\dot{y}_0^+ \exp[-\zeta_1\omega_1(1+\mu)t]\sinh\left(\sqrt{\zeta_1^2(1+\mu)^2-(1+\mu)}\,\omega_1 t\right)}{\sqrt{\zeta_1^2(1+\mu)^2-(1+\mu)}\,\omega_1}, & \zeta_1\sqrt{1+\mu} > 1 \end{cases} \tag{25}$$

Furthermore, for conveniently analyzing the effect of the impact mass, use $\beta = \zeta_1\sqrt{1+\mu}$, $\omega_n = \omega_1\sqrt{1+\mu}$ and introduce the variables $\gamma = \arccos\beta$ and $\gamma' = \operatorname{arccosh}\beta$ to represent the damping ratio β for the analysis of the underdamped and the overdamped cases of the motion. The solutions for the two cases $\beta < 1$ and $\beta > 1$ can be unified using the relationship $\gamma' = j\gamma$. Here, the variable γ decreases from $\pi/2$ to zero as the damping ratio increases from zero to unity, and the second variable γ' increases from zero to infinity as the damping ratio increases beyond unity.

By setting $\ddot{y} = 0$, the contact force can be expressed as $-m\ddot{y}/(1+\mu)$, and consequently, $\ddot{y}$ vanishes at the end of the impact. The duration time of impact can be evaluated as (Eberhard and Hu, 2003)

$$\tau = \begin{cases} 2\gamma/\omega_n \sin\gamma, & \beta < 1 \\ 2\gamma'/\omega_n \sinh\gamma', & \beta > 1 \end{cases} \tag{26}$$

For the critically damped case, the variables γ and γ' vanishing, and consequently the duration of impact of $\beta = 1$ can be deduced from the limit of the right hand side of equation as $2/\omega_n$. By imposing $\dot{y} = 0$, the time taken for the compression in the spring–damper combination to reach its maximum value can be obtained from Eqs. (25) and (26) as $\tau/2$. The relative velocity of separation $\dot{y}_0^-$ of the masses after the impact is determined from Eq. (25) as the value of $-\dot{y}$ at $t = \tau$. Based on Eq. (4), the coefficient of restitution, $\alpha = \dot{y}_0^+/\dot{y}_0^-$, is then evaluated as

$$\alpha = \begin{cases} \mathrm{e}^{-2\gamma/\tan\gamma}, & \beta < 1 \\ \mathrm{e}^{-2\gamma'/\tanh\gamma'}, & \beta > 1 \end{cases} \tag{27}$$

From the definitions of γ and γ', it can be seen that the expression for the coefficient of restitution in Eq. (27) depends on the damping ration β only. For the critically damped case, the limiting value of the right

hand side of Eq. (27) yields the coefficient of restitution as e^{-2}. Eqs. (26) and (27) are shown graphically in Figs. 4 and 5 as variation of the coefficient of restitution α and the non-dimensional impact duration $\omega_n\tau$ against the damping ratio β. Fig. 4 indicates that the coefficient of restitution is a monotonically decreasing function of the damping ratio. In Fig. 5, the variation of the non-dimensional impact duration is a monotonically decreasing function of the damping ratio. These graphs may be used to estimate the values of β and ω_n from α and τ. Figs. 4 and 5 can also be used to determine α and τ from known values of values of β and ω_n. Thus, the impact duration is an important parameter similar to the coefficient of restitution, which depends on the material and surface condition of impacting bodies. Specially, this observation implies that the impact duration is independent of the velocities of the impacting bodies. Since $k = m\omega_n^2$, the parameters of the contact spring–damper combination can be determined from the impact duration, coefficient of restitution and the reduced mass m.

For considering the influence of the clearance d, it is non-dimensionalized with the root mean square (RMS) amplitude without impact damper as d/A_0. The RMS amplitude A_{rms} is defined as $A_{\text{rms}} = \left(\frac{1}{T}\int_0^T A^2(t)\mathrm{d}t\right)^{1/2}$, where T is the observation period and $A(t)$ is the amplitude of the displacement. The simulative results are shown in Fig. 6. A reduction of the RMS amplitude of the main mass of about 70% can be observed over a wide range of clearances. The introduction of the impact damper clearly enhances the effectiveness of the lightly damped absorber for clearances over $d/A_0 = 10$.

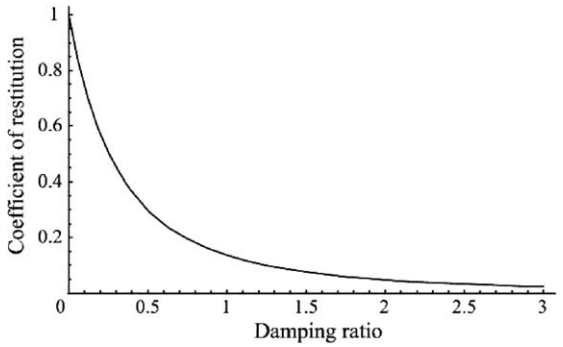

Fig. 4. Variation of coefficient restitution with damping ratio.

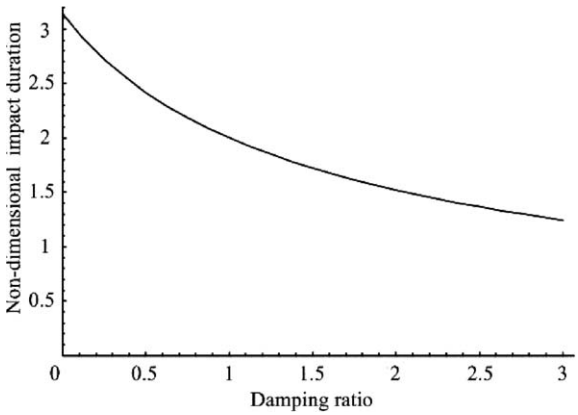

Fig. 5. Variation of impact duration with damping ratio.

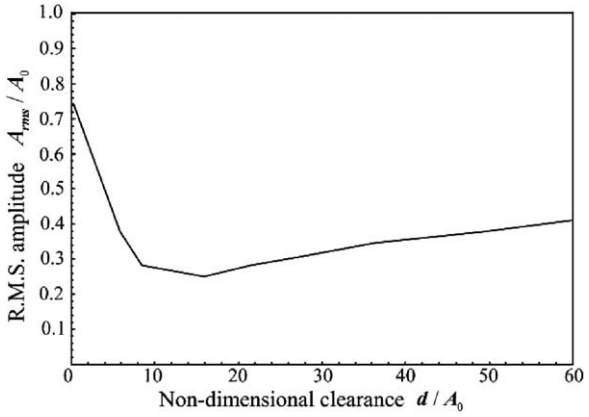

Fig. 6. The RMS amplitude responses versus impact clearance.

4. Application of an impact damper to a rotating cantilever beam

In this section, we consider how the proposed designs for semi-active vibration impact damper can be extended to the vibration control of cantilever beam. Use a uniform, Bernoulli–Euler beam of length l, cross-sectional area S, Young's modulus E, density ρ, lying in the x–y plane with one end fixed and the other free. An impact damper that situated on the inner of beam has a free mass m at $x = x_0 = 0.59$ m as shown in Fig. 7. In Fig. 8 shown an experimental test frame and relevant parameters as Table 1. The data recording equipment is the HP35670A dynamic signal analyzer.

The impact interface is characterized by an equivalent spring constant K_I and damping constant C_I. The friction can be neglected because the clearance between the impact mass and the cantilever beam is very small. Motion equations of the rotating cantilever beam and the impact damper can be expressed as follows:

Case I: When $W(x_0,t) - V(t) \leqslant 0$, the impact damper collides with the beam at right side, whereas $W(x_0,t) - V(t) \geqslant \Delta$, the impact mass collide with the beam at the left side. The equation of motion is the same in either situation and is expressed as

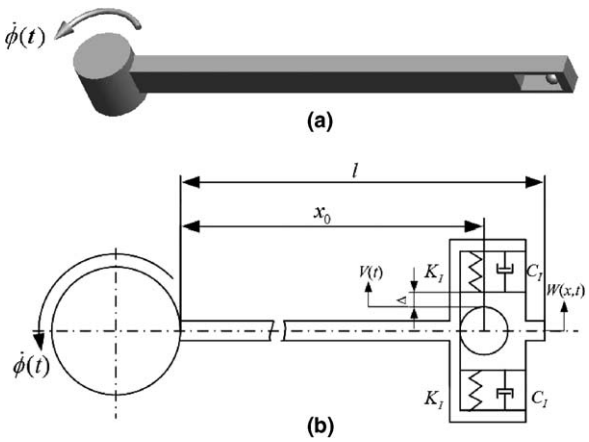

Fig. 7. (a) Schematic diagram of model; (b) top view of impact damper in cross section.

Fig. 8. The experimental test frame and partial impact damper structure.

Table 1
Parameters for the cantilever beam and impact damper

Cantilever beam	Impact damper
Length, $l = 0.6$ m	$m = 2.1 \times 10^{-3}$ kg
Density, $\rho = 2.7 \times 10^3$ kg/m^3	$C_I = 20$ N s/m
Young's modulus, $E = 7 \times 10^{10}$ N/m^2	$K_I = 0.8 \times 10^5$ N/m
Cross-sectional area, $S = 3.6 \times 10^{-4}$ m^2	
Cross-sectional second moment of area, $I = 2.7 \times 10^{-8}$ m^4	

$$m\frac{\mathrm{d}^2V(t)}{\mathrm{d}t^2} = -C_{\mathrm{I}}\left(\frac{\mathrm{d}V(t)}{\mathrm{d}t} - \frac{\partial W(x_0,t)}{\partial t}\right) - K_{\mathrm{I}}[V(t) - W(x_0,t)] \tag{28}$$

$$EI\frac{\partial^4 W(x,t)}{\partial x^4} + \rho S\frac{\partial^2 W(x,t)}{\partial t^2} = C_{\mathrm{I}}\left(\frac{\mathrm{d}V(t)}{\mathrm{d}t} - \frac{\partial W(x_0,t)}{\partial t}\right) + K_{\mathrm{I}}[V(t) - W(x_0,t)] + \left[\dot{\phi}(t)\right]^2\left\{(l-x)\left(a+\tfrac{1}{2}(l+x)\right)\frac{\partial^2 W(x,t)}{\partial x^2} - (a+x)\frac{\partial W(x,t)}{\partial x}\right\} \tag{29}$$

where $W(x_0,t)$ is the displacement of the cantilever beam measured at $x = x_0$, $V(t)$ is the displacement of the impact mass.

Case II: When $0 \leqslant W(x_0,t) - V(t) \leqslant \Delta$, the impact mass moves freely at a constant speed causing any collision of motion is given by

$$EI\frac{\partial^4 W(x,t)}{\partial x^4} + \rho S\frac{\partial^2 W(x,t)}{\partial t^2} = \left[\dot{\phi}(t)\right]^2\left\{(l-x)\left(a+\tfrac{1}{2}(l+x)\right)\frac{\partial^2 W(x,t)}{\partial x^2} - (a+x)\frac{\partial W(x,t)}{\partial x}\right\} \tag{30}$$

$$V(t) = \dot{V}_0 t + V_0 \tag{31}$$

where $\dot{V}_0$ and V_0 are the respective velocity and displacement while the impact damper separates from the beam.

The beam displacement $W(x,t)$ is solved using the assumed mode method

$$W(x,t) = \sum_{i=1}^{\infty}\psi_i(x)\eta_i(t) \tag{32}$$

where $\eta_i(t)$ is the modal displacement and $\psi_i(x)$ is the eigenfunction expressed as follows for a cantilever beam:

$$\psi_i(x) = \cosh(k_i x) - \cos(k_i x) - r_i[\sinh(k_i x) - \sin(k_i x)] \tag{33}$$

where k_i is the ith dimensionless frequency parameter found from the solution of the transcendental frequency equation

$$\cos k_i \cosh k_i + 1 = 0$$

and r_i is a weighting constant associated with each mode, defined as

$$r_i = \frac{\sin(k_i l) - \sinh(k_i l)}{\cos(k_i l) + \cosh(k_i l)}$$

For simplified analysis, we consider the free vibration of beam in the halted state, i.e., $\dot{\phi}(t) = 0$. Now, Eq. (32) substituted into Eq. (29), the result is yielded as

$$\begin{aligned} V(t) = \left(\frac{1}{m\omega_{\mathrm{Id}}}\right) \int_0^t \left[\sum_{i=1}^{\infty} \psi_i(x_0)(C_{\mathrm{I}}\dot{\eta}_i(\tau) + K_{\mathrm{I}}\eta_i(\tau))\right] \sin\left[\omega_{\mathrm{Id}}(t-\tau)\right] \mathrm{d}\tau + V_0 \exp(-\xi\omega_{\mathrm{In}} t) \\ \times \cos(\omega_{\mathrm{Id}} t) + (1/\omega_{\mathrm{Id}})(\dot{V}_0 + \xi\omega_{\mathrm{In}} V_0) \exp(-\xi\omega_{\mathrm{In}} t) \sin(\omega_{\mathrm{Id}} t) \end{aligned} \tag{34}$$

where $\omega_{\mathrm{Id}} = \omega_{\mathrm{In}}\sqrt{1-\xi^2}$, $\omega_{\mathrm{In}} = \sqrt{K_{\mathrm{I}}/m}$, $\xi = \frac{C_{\mathrm{I}}}{2\sqrt{K_{\mathrm{I}} m}}$. V_0, $\dot{V}_0$ are the initial displacement and the initial velocity.

Substituted Eq. (33) into Eq. (30) and applied the orthogonality of the modal functions, the modal displacement is then obtained by solved as follows the differential equation

$$\ddot{\eta}_i + \frac{C_{\mathrm{I}}}{\rho S}\dot{\eta}_i + \left(\omega_i^2 + \frac{K_{\mathrm{I}}}{\rho S}\right)\eta_i = C_{\mathrm{I}}\dot{V}(t) + K_{\mathrm{I}} V(t), \tag{35}$$

where $\omega_i^2 = \frac{\int_0^l EI(\psi_i''(x))^2 \mathrm{d}x}{\int_0^l \rho S(\psi_i(x))^2 \mathrm{d}x}$, the derivatives with respect to t and x are denoted by $(\cdot)$ and $()'$, respectively.

The data in Table 1 are substituted into Eqs. (34) and (35), in $x = x_0 = 0.59m$, and the vibration response of cantilever beam can be approximately obtained as follows:

$$\begin{aligned} W(x_0, t) = 2A[\mathrm{e}^{-4.465t}\sin(138.2t + \phi) + \mathrm{e}^{-28.31t}\sin(876.5t + \phi)] + \mathrm{e}^{-4752t}[(-13.95 \times 10^{-7}\dot{V}_0 \\ - 0.0084 V_0)\cos(3938t) + (-5.08 \times 10^{-7}\dot{V}_0 + 0.00343 V_0)\sin(3938t)] \end{aligned} \tag{36}$$

where $A = \sqrt{\eta_0^2 + (\frac{\dot{\eta}_0 + 4.464\eta_0}{138.13})^2}$, $\phi = \tan^{-1}\frac{138.13\eta_0}{\dot{\eta}_0 + 4.464\eta_0}$.

The vibration response of numerical simulation is shown in Fig. 9(a). The time history of experimental result is recorded in Fig. 9(b). From Fig. 9, the numerical and experimental results basically coincide with each other. Both damping ratios are nearly equal. The deflections of both results mainly are caused by the computation error, since the higher order mode functions are not taken into account. The natural frequency of the second mode is over six times higher than that of the first mode.

In Fig. 10, the frequency responses of the experimental system are recorded, when Fourier transformation and averaging algorithm are adopted by the dynamic signal analyzer. The frequency responses of the displacement at beam end are presented in Fig. 10(a)–(d). Fig. 10(a) shows a beam without impact damper. Fig. 10(b)–(d) demonstrate the impact damper third different positions placed at, $x_0 = 10{,}590{,}300$ mm, respectively. The vibration detector locates on the beam end. It is clear that the amplitude is higher without the impact damper (see Fig. 10(a)). When the impact mass locates the root of beam, the effectiveness of reducing vibration is very feeble (see Fig. 10(b)). The impact mass situating at higher amplitude point of beam, can increase the velocity and number of impacts, so that several impacts can be observed on the same

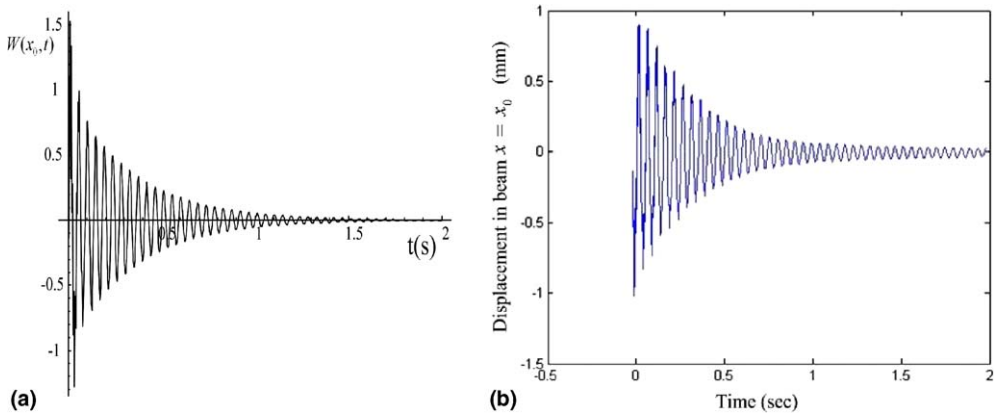

Fig. 9. Compared two responses of the beam with impact damper. (a) The result of numerical simulation; (b) experimental result.

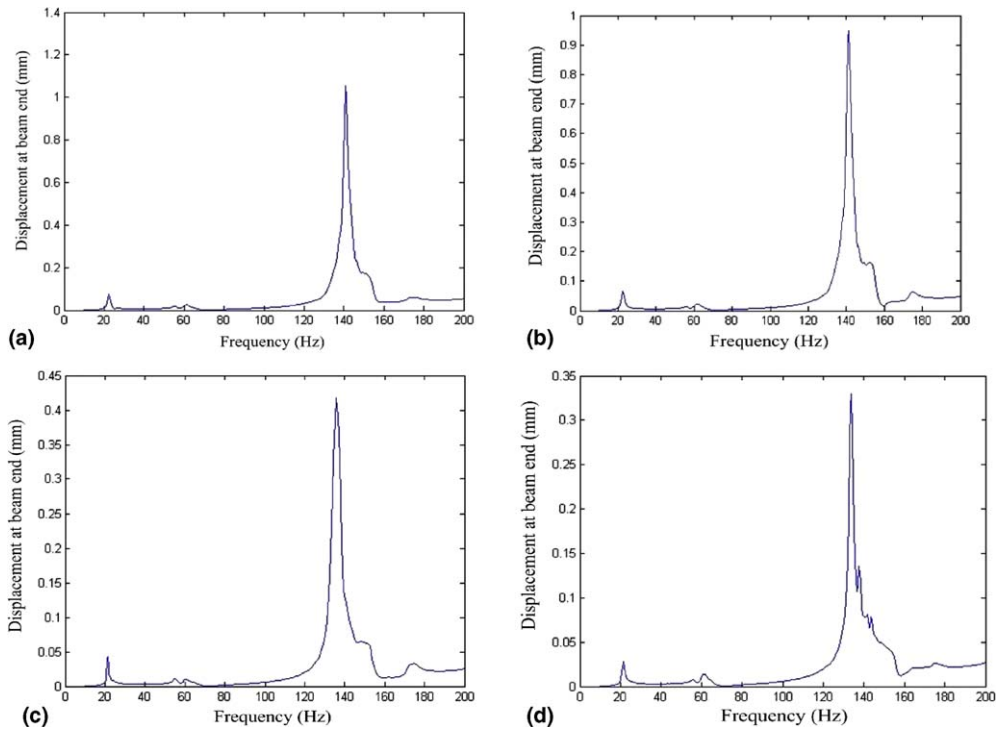

Fig. 10. The experimental frequency responses of the displacement at beam end the mass damper placed at the different position of beam (a) without; (b) $x_0 = 10$ mm; (c) $x_0 = 590$ mm; (d) $x_0 = 300$ mm.

side before collision with the opposite side. The control effectiveness from the momentum transfer between impact damper and beam is thereby deteriorated (see Fig. 10(d)). Compared between Fig. 10(a) and (d), the effect of decreasing vibration is very evident, the measured decreasing amplitude reaches up to 70%. It is clear that the impact damper is effective to suppress the excessive vibration of beam in high-frequency range.

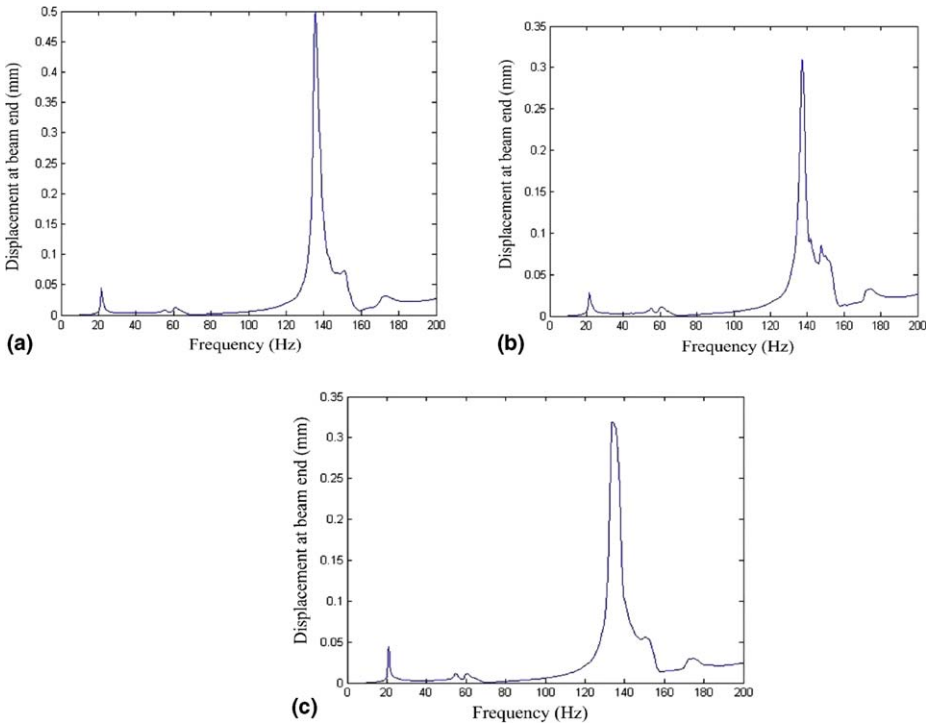

Fig. 11. The experimental frequency responses of the displacement at beam end applied the mass damper with different liquid in clearance.

In Fig. 11, we add the viscous liquid to impact clearance for increasing the damping ratio and eliminating the high resonance produced by the impact. Fig. 11(a) show without liquid in clearance, the damping ratio of beam vibration is thereby smaller estimated at 0.05. With water in impact clearance, the damping ratio estimated at 0.12 by the analyzer analyzing (see Fig. 11(b)). The frequency response of displacement is lower than ones without the liquid. In Fig. 11(c), the damping ratio approximately comes to 0.2 with viscous silicone oil, but the displacement reducing inconspicuously. To apply viscous liquid, therefore, it can validate to eliminate the high-frequency resonance by impact producing.

5. Conclusion

This paper presents new analytical results for applying the impact damper reducing structure vibration. The explicit analytical results provide insight into the complex relationships between the properties of the impact damper and the state of the system. The results lead directly to closed expressions for the optimal initial displacements and state-dependent impact damping. The optimal initial displacement is a monotonically increasing function of damping. The exponential decay rate of the main mass response is proportional to both the optimal initial displacement and the mass ratio. The duration of impact is taken into account. This feature is important for a resilient rather than a rigid impact damper is used when the noise issue is considered. The results clearly show that the reduction of the vibration response does not depend on the number of impacts, but primarily on the collision that occurs while the impact mass and the main mass are moving toward each other.

The theory is strictly developed for single-degree-of-freedom structures, and the theory also applied to continuous structures with widely range of natural frequencies. In case of imprecise model, a simpler, less sensitive control algorithm for the state-dependent damping also comes into effect. With the aid of practical testing, the effectiveness of vibration attenuation is evident to apply the impact mass in cantilever beam. The result of theoretical analysis agrees with the experimental one. Simultaneously, the viscous liquids that permeate in impact clearance enable to eliminate the high-frequency resonance produced by the impact action.

Acknowledgement

This work is supported by the National Nature Science Foundation of China (No. 10372076), for which the authors are grateful.

References

Barbara, B.-O., 2001. Analysis of an impact damper of vibrations. Chaos, Solitons and Fractals 12, 1983–1988.

Carotti, A., Turci, E., 1999. A tuning criterion for the inertial tuned damper. Design using phasors in the Argand–Gauss plane. Applied Mathematical Modelling 23, 199–217.

Cheng, C.C., Shiu, J.S., 2001. Transient vibration analysis of a high speed feed drive system. Journal of Sound and Vibration 239 (3), 489–504.

Cheng, C.C., Wang, J.Y., 2003. Free vibration analysis of a resilient impact damper. International Journal of Mechanical Science 45, 589–604.

Collette, F.S., 1998. A combined tuned absorber and pendulum impact damper under random excitation. Journal of Sound and Vibration 216 (2), 199–213.

Dlmentberg, M.F., Iourtchenko, D.V., 2004. Random vibrations with impacts: a review. Nonlinear Dynamics 36, 229–254.

Eberhard, P., Hu, B., 2003. Advance Contact Dynamics. Southeast University Press, China.

Ema, S., Marui, E., 1996. A fundamental study on impact dampers. International Journal of Machine Tools and Manufacturers 36 (3), 293–306.

Fujino, Y., Abe, M., 1993. Design formulas for tuned mass dampers based on a perturbation technique. Earthquake Engineering and Structural Dynamics 22, 833–854.

Igusa, T., Der Kiureghian, A., 1985. Dynamic characterization of two-degree-of-freedom equipment-structure systems. Journal of Engineering Mechanics 111, 1–19.

Janin, O., Lamarque, C.H., 2001. Comparison of several numerical methods for mechanical systems with impacts. International Journal for Numerical Methods in Engineering 51, 1101–1132.

Joshi, A.S., Jangid, R.S., 1997. Optimum parameters of multiple tuned mass dampers for base-excited damped systems. Journal of Sound and Vibration 202 (5), 657–667.

Lamarque, C.H., Janin, O., 2000. Modal analysis of mechanical systems with impact non-linearities: limitations to a modal superposition. Journal of Sound and Vibration 235 (4), 567–609.

Wang, J.F., Lin, C.C., Chen, B.L., 2003. Vibration suppression for high-speed railway bridges using tuned mass dampers. International Journal of Solids and Structures 40, 465–491.

Yao, W.L., Chen, B., Liu, C.S., 2005. Energetic coefficient of restitution for planar impact in multi-rigid-body systems with friction. International Journal of Impact Engineering 31, 255–265.

Zhang, D., Angeles, J., 2005. Impact dynamics of flexible-joint robots. Computers & Structures 83, 25–33.